JOURNAL OF SPACECRAFT AND ROCKETS
Vol. 47, No. 2, March–April 2010

Plasma Torch Test of an Ultra-High-Temperature Ceramics Nose Cone Demonstrator

L. Scatteia,* D. Alfano,† and S. Cantoni‡
Centro Italiano Ricerche Aerospaziali, 81043 Capua, Italy
F. Monteverde§
National Research Council, 48018 Faenza, Italy
and
M. De Stefano Fumo¶ and Andrea Di Maso**
University of Naples "Federico II," 80125 Napoli, Italy

DOI: 10.2514/1.42834

An ultra-high-temperature ZrB_2–SiC ceramic nose cone was tested in an arcjet plasma torch facility for 10 min at temperatures above 2000°C. The nose cone model was obtained from a hot-pressed billet via electrical discharge machining. The relevant portions of the models directly exposed to the hot stream were analyzed by scanning electron microscopy and energy-dispersive spectroscopy. The posttest cross sectioning of the model showed a nonnegligible surface recession on the tip of the nose. Nonetheless, the material exhibited a promising potential to withstand severe reentry conditions with temperatures exceeding 2000°C in a single-use application. Spectral directional emissivity evaluations were performed on the fly during the test by means of thermography coupled with dual-color pyrometer. The numerical calculations, which simulated the chemical nonequilibrium flow around the model assuming a low catalytic surface behavior, are in good accordance with the experimental results.

Nomenclature

D	=	diffusion coefficient, $m^2\ s^{-1}$
Kw	=	catalytic recombination constant, $m\ s^{-1}$
M	=	the molecular weight, $g\ mol^{-1}$
$\bar{n}$	=	unit vector normal to the wall
R_0	=	gas law constant, $J\ mol^{-1}\ K^{-1}$
T_w	=	wall temperature, K
α	=	the atomic composition
β	=	accommodation energy
γ	=	catalytic efficiency
γ'	=	accommodation coefficient
δ	=	density, $g\ cm^{-3}$
ε	=	emissivity
λ	=	wavelength, μm
μ	=	kinematic viscosity, $kg\ m^{-1}\ s^{-1}$
ρ	=	density, $kg\ m^{-3}$

Subscripts

t	=	turbulent
w	=	wall conditions

Received 18 December 2008; revision received 8 October 2009; accepted for publication 22 October 2009.

*Researcher, Advanced Materials and Manufacturing Department, Via Maiorise; l.scatteia@cira.it.
†Researcher, Advanced Materials and Manufacturing Department, Via Maiorise; d.alfano@cira.it.
‡Researcher, Advanced Materials and Manufacturing Department, Via Maiorise; s.cantoni@cira.it.
§Researcher, Institute of Science and Technology for Ceramics, Via Granarolo 64; fmonte@istec.cnr.it.
¶Research Assistant, Department of Aerospace Engineering, Piazzale Tecchio 80; madestef@unina.it. Member AIAA.
**Ph.D. Student, Department of Aerospace Engineering, Piazzale Tecchio 80; dimasoandrea@email.it.

I. Introduction

CERAMIC compounds based on metal borides, such as zirconium diboride (ZrB_2) and hafnium diboride (HfB_2), are usually defined as ultra-high-temperature ceramics (UHTC) for their extremely high melting temperatures. Compared to HfB_2, ZrB_2 has a lower theoretical density ($6.10\ g\ cm^{-3}$) [1,2], which makes it much more attractive for aerospace applications, such as sharp-leading-edge hot structures on future generations of slender-shaped reentry vehicles [3–6]. Actually, the highly thermal demanding trajectories foreseen for future space-plane-like winged reentry vehicles dictate the need of designing materials able to sustain not only operating temperatures approaching 2200°C but also to resist evaporation, erosion, and oxidation in the harsh reentry environment.

Because UHTC were thus far produced only in monolithic, sintered form, they exhibit the typical low thermal shock resistance of monolithic ceramics and are therefore presently suitable only for the manufacturing of small components or parts of nose cones and leading edges: this poses the issue of mechanical interfaces with backstructures and high backwall temperatures (the issue being even more critical due to the high thermal conductivity of this class of compounds). Even though conspicuous efforts are being devoted to reach these objectives by the Italian Aerospace Research Centre and the Italian Space Agency in dedicated technological projects at the state and mainly for the aforementioned issues, an in-flight demonstration of a UHTC-based hot structure (intending a load-bearing thermal structure that includes mechanical interfaces with colder structures) has yet to be conducted, although, in-flight experiments on UHTC specimens were performed in the past decade by NASA Ames in the framework of the scientific projects SHARP B1 and B2 [7] and Delta Clipper (DC-X and DC-XA) [8].

However, UHTC compounds are generally characterized by a far superior oxidation resistance at ultrahigh temperatures (that is, above 2000°C), with respect to conventional SiC-based ceramic matrix composites, and, as such, they can still be considered a promising class of thermal protection system (TPS) materials worthy of investigation in order to foster the step ahead that is presently needed to overcome the limitation of currently employed ceramic TPS.

Pure ZrB_2 has a poor oxidation resistance in air above 1200°C because of rapid volatilization of boria (B_2O_3), which results in the formation of a porous and scarcely protective external ZrO_2 layer [6,9–12]. For oxidation environment at total pressure well below

Table 1 Some characteristics of the raw powders: specific surface area (obtained by the Brunauer, Emmett, and Teller method) and particle size range (obtained by SEM).

	Company	Type	Specific surface area, m^2/g	Particle size range, μm	Main impurities[a], wt %
ZrB_2	H.C. Starck, Goslar, Germany	Grade B	1	0.2–10	O:1 and Hf:0.2
SiC	H.C. Starck, Goslar, Germany	BF12	11.6	0.05–2	O:1.65

[a]From suppliers.

1 atm, the volatility of boria increases with the consequential reduction of the oxidation resistance of pure zirconium diboride [5,13]. The addition of 10 to 30 vol % SiC proved to be an effective way to improve the oxidation resistance between 1200 and 1600°C, thanks to the formation of less volatile external silica-rich glassy coatings [5,6,11,12,14–19], which act as an effective barrier to oxygen diffusion. This makes the ZrB_2–SiC system very attractive for the aforementioned application.

The past decade has seen the publication of a large number of works focused on the ZrB_2–SiC-based UHTC as hot structure materials. However, very few data are available on UHTCs exposed at temperatures exceeding 2000°C and for significant durations (more than 5 min) [20,21].

The objective of this paper is to report on a long-duration, ultra-high-temperature plasma torch exposure test performed on a UHTC nose cone demonstrator. The UHTC constituting the nose cone demonstrator is based on a ZrB_2–SiC system developed within the Sharp Hot Structures project (a technology project within the Italian Unmanned Space Vehicle program) [22,23]. This material was fully characterized in its thermomechanical properties [24,25] as well as in its surface properties and oxidation in laboratory-scale tests [26,27].

The ceramic nose cone was machined out of a hot-pressed billet by electrical discharge machining (EDM) and then exposed to a plasma torch for more than 10 min at temperatures higher than 2000°C. The hold at the maximum temperature of 2300°C lasted about 2 min. A detailed microstructure investigation was performed on the portions of the nose cone more heavily exposed to the hot plasma jet in order to evaluate the overall performance of the base material under long-duration exposure at ultrahigh temperatures.

II. Experimental

A. Material

The nose cone demonstrator was obtained by a hot-pressed cylinder of ZrB_2 + 15 vol % SiC. The cylinder was obtained by hot pressing. The powder mixture was wet-mixed in absolute ethyl alcohol using SiC milling balls and was further dried with a rotary evaporator under a continuous stream of inert gas. As a sintering aid, a small amount of $MoSi_2$ (2 vol %) was batched into the initial powder mixture. ZrB_2 and β-SiC raw powders were from H. C. Starck, while $MoSi_2$ from Sigma-Aldrich. In Table 1, some characteristics of the used powders are summarized. The final sintered material has a density of 5.610 g/cm^3.

B. Nose Cone Manufacturing

The nose cone ceramic demonstrator was shaped by EDM from the hot-pressed cylinder. The maximum diameter and the height of the electrical discharge machined article are 5.5 and 7.0 cm, respectively. The tip of the nose cone is a half-sphere characterized by a radius of curvature of 1.0 cm. In the base of the nose cone, a cylindrical hole was made by EDM in order to mount the article on the cylindrical sample holder inside the controlled atmosphere plasma spray (CAPS) test chamber during the plasma torch test. The hole is 2.2 cm deep and has a diameter of 1.69 cm.

C. Test Facility

The CAPS facility, located at Centro Sviluppo Materiali (Rome), was used for the plasma exposure test. The facility is equipped with a Sulzer Metco F4-MB plasma gun that can be operated with combinations of argon, hydrogen, and helium up to power levels of 55 kW. Special nozzles are available to operate also with nitrogen. An automatic control system monitored the main parameters of the apparatus (voltage and current of the arc heater, water cooling temperature, and mass flow rate). In particular, the specific total enthalpy H was evaluated through an energy balance between the energy supplied to the gas by the arc heater and the energy transferred to the cooling system (measured by the water temperature jump between inlet and outlet).

The present test has been carried out with an argon–nitrogen mixture (argon at 74 wt %) with mass flow rate of 1.46 g/s. Beyond the nozzle, the high-temperature gas reacts with cold air and evolves in a mixture of Ar, atomic and molecular nitrogen, and atomic and molecular oxygen (neglecting the ionization phenomena in our analysis), as stated in Sec. IV. The aerothermochemical environment during the test is therefore similar to those surrounding reentry vehicles, at least for atomic and molecular oxygen compositions, which are the main species affecting the oxidation and erosion process of the UHTC specimen. The torch power varies from 38.3 to 63.7 kW during the test, which corresponds to an average specific total enthalpy of the flow at the torch exit, varying from 8 to 22 MJ/kg at atmospheric pressure, resulting in subsonic flow regime. Similar tests have been carried out by some of the authors of the present paper in another facility available at the Department of Aerospace Engineering of the University of Naples on small scale (hemispherical and conical models), both at subsonic and supersonic

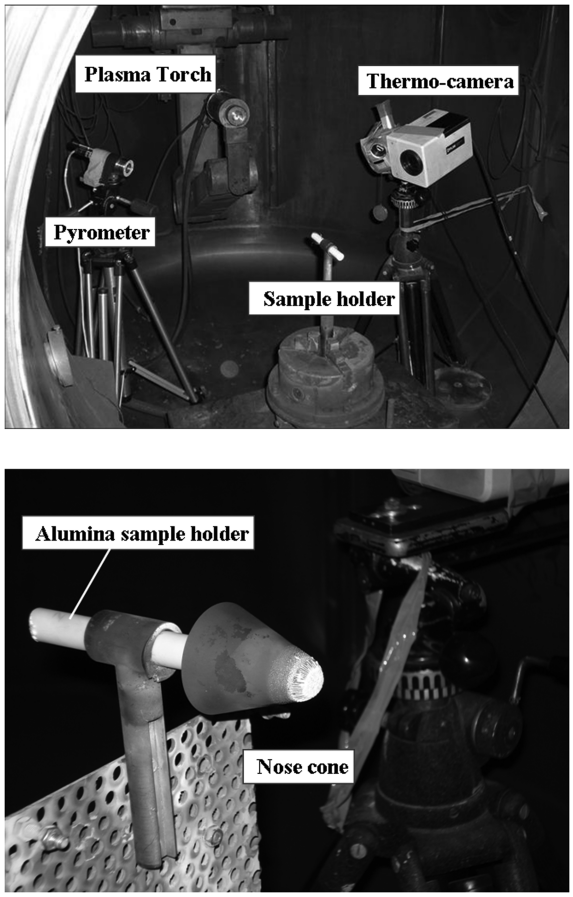

Fig. 1 The experimental setup used for the exposure test, installed within the CAPS test chamber (top), and the nose cone fixed at the alumina sample holder after the plasma test (bottom).

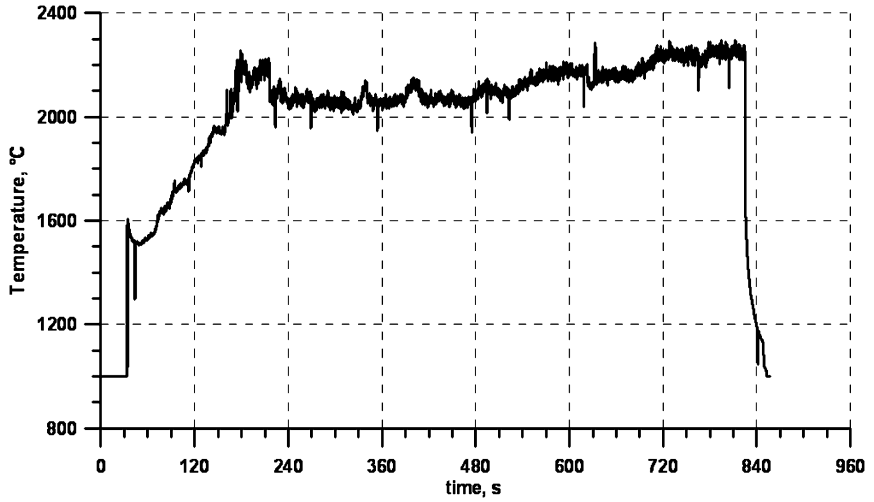

Fig. 2 Surface temperature vs time during the test: temperatures in excess of 2000°C were reached on the tip of the nose cone for more than 10 min of exposure time.

conditions ($M = 3$) on different material compositions. During the supersonic tests, the stagnation point achieves about 0.1 atm with a mixture of nitrogen and oxygen (the oxygen is fed by a swirling mixer after the torch and before a convergent–divergent nozzle) [28,29].

D. Test Procedure

The surface temperature of the nose cone was measured with the radiation ratio pyrometer (IMPAC ISQ 5). In two-color mode, the instrument makes use of the ratio of two spectral radiances measured at 0.92 and 1.05 μm to evaluate the true temperature overcoming the problem of the emissivity knowledge. In combination with the pyrometer, the infrared thermocamera FLIR SC3000 is used to measure the surface-temperature distributions and the local spectral emissivity of the material at the measurement spot of the pyrometer in the longwave range of the thermograph ($\lambda = 9$ μm). The test article was mounted on an alumina cylindrical sample holder and kept at a distance of 6 cm from the exit nozzle (see Fig. 1).

The test was conducted by manually tuning the plasma torch power in order to get the desired test temperature on the test article. The test was conducted at ambient air pressure because the CAPS test chamber was kept open in order to accommodate the optical instrumentation inside.

Because of the complexity of the test geometry, only one nose cone sample was produced, and because the surface modification occurred after the test and the need to perform destructive microstructural analysis on the affected region, no test repetition was conducted.

E. Posttest Microstructural Analyses

Posttest microstructural analyses of relevant transversal cross sections of the nose cone tip were conducted with a scanning electron microscopy (SEM, Leica Cambridge S360) equipped with an energy-dispersive microanalyzer (EDS, INCA Energy 300, Oxford Instruments). The transversal sections were polished with diamond pastes down to 0.25 μm and then observed by SEM–EDS. The as-prepared polished cross sections were coated with a thin carbon layer.

III. Results and Discussion

A. Real-Time Emissivity Measurements

In Fig. 2, the time-vs-temperature profile related to surface of the tip of the nose measured with the dual-color pyrometer is shown. During the first 3 min, the temperature of the nose cone's tip rapidly increases up to 2200°C. Then, the temperature decreased to 2100°C and remained at this value for about 6 min. For the last 4 min, the temperature increased slowly up to the maximum measured temperature of 2300°C.

Once the temperature is measured with the pyrometer and the instrument is switched to the single-color mode, the spectral radiance at the wavelength of 0.92 μm is measured and this value, together with the known temperature value, is used to evaluate the spectral emissivity. The directional and spectral emissivity value at $\lambda = 9$ μm of about 0.9 was estimated.

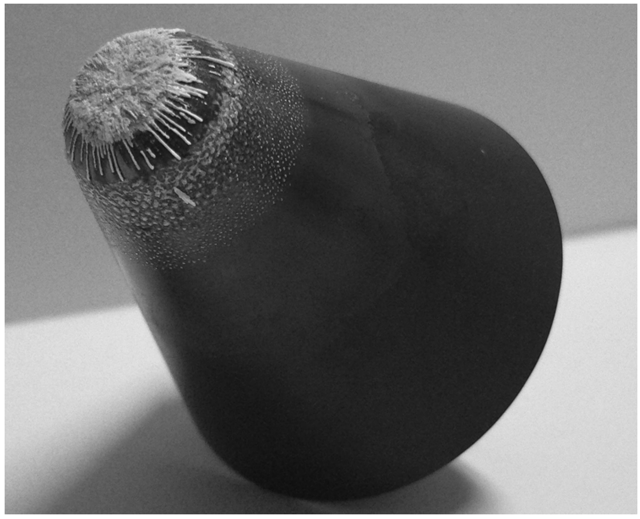

Fig. 3 The nose cone after high-temperature plasma exposure.

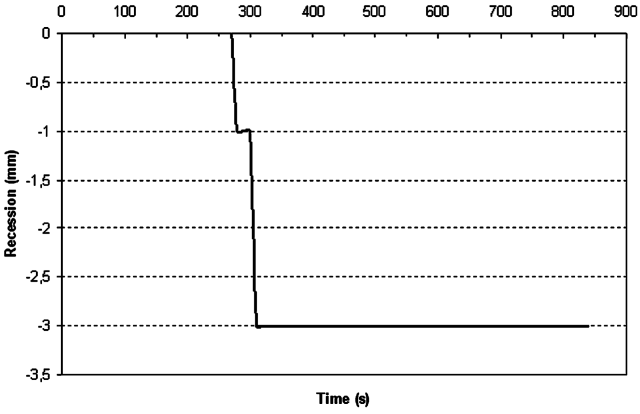

Fig. 4 Stagnation-point recession during the test (estimated via image analysis on the recorded thermography).

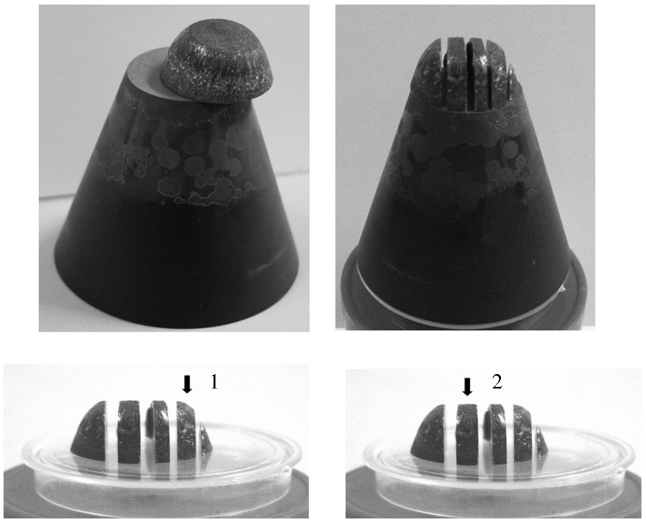

Fig. 5 The nose cone after the removal of the surface deposit and radial cut (left) and after the subsequent transversal cross section cut: optical pictures of the transversal cross sections referred to as no. 1 and no. 2.

B. Posttest Microstructural Analysis

In Fig. 3, the nose cone after the exposure test is shown. The formation of a nonadherent, crumbly deposit on the tip was evident. This deposit was easily removed from the bulk material, pulverized, and then analyzed by x-ray defraction: the only identified crystalline phase was monoclinic zirconia. The SEM–EDS chemical analysis of the pulverized deposit confirmed the presence of only Zr and O.

During exposure, a certain amount of molten oxidation products was blown away and resulted in an apparent erosion of the pristine profile (see Fig. 3). The graph in Fig. 4 depicts the stagnation-point regression because of the exposure, estimated roughly via image analysis on the thermography recorded during the test. This estimation shows a total regression of the stagnation point of about 3 mm during the entire test.

Significant oxidation coupled with erosion took place in those regions directly exposed to the hot flux. No solid Si-containing oxides resisted but evolved into volatile products, such as gaseous SiO and SiO_2, which have vapor pressure that is no longer negligible at these very high temperatures [17,21,30–34].

Increasing the surface temperature above 2200°C, the as-formed surface oxide products tended also to soften and deform under the influence of the high shear stresses connected to the hot gas flow. This resulted in the formation of recrystallized zirconia filaments (see Fig. 3) in colder portions of the nose cone tip. It should also be noted that softening and erosion of this zirconia-based oxide deposit was also influenced by the formed SiO_2 and B_2O_3, determined, respectively, by the oxidation of SiC and ZrB_2. The final effect of this massive oxidation of the ZrB_2–SiC composites was an apparent weight loss of 7% associated with the loss of the original spherical profile of its tip (see Fig. 3).

Figure 5 shows the nose cone after the removal of the surface deposit and the radial cut (first picture on the left) and after the subsequent transversal cross sections cut. From the cross sections cut, two sections referred to as no. 1 and no. 2 were taken and polished for SEM–EDS analysis.

In Fig. 6, the SEM micrographs of cross sections 1 and 2 are compared. Both sections show a residual outermost layer consisting of a silica-based glassy layer in regions relatively far from the eroded pristine tip. The thicker external glassy scale of section 1 could be explained, considering that section 2 is closer to the longitudinal axis of the nose cone tip in which the heat-flux values were much higher than for section 1. In section 1, the stronger shear forces associated with the higher-heat fluxes aid the erosion processes with the consequential formation of recrystallized zirconia filaments. Considering that a zirconia-based layer alone is not effective as a barrier for the oxygen diffusion [6,9–13], in correspondence with the regions underlying the original locations of the zirconia filaments, the oxidation of the composite proceeded faster, actually involving deeper layers of the nose tip. The SEM observation of the transversal section 1 shows that the reacted regions underneath the longitudinal trails are wider and deeper with respect to the remaining areas of the section (see Fig. 7) and much less protected compared to other zones still covered by an adherent silica-based glassy coating. The protective coverage of a silica glassy layer apart, the very-high-

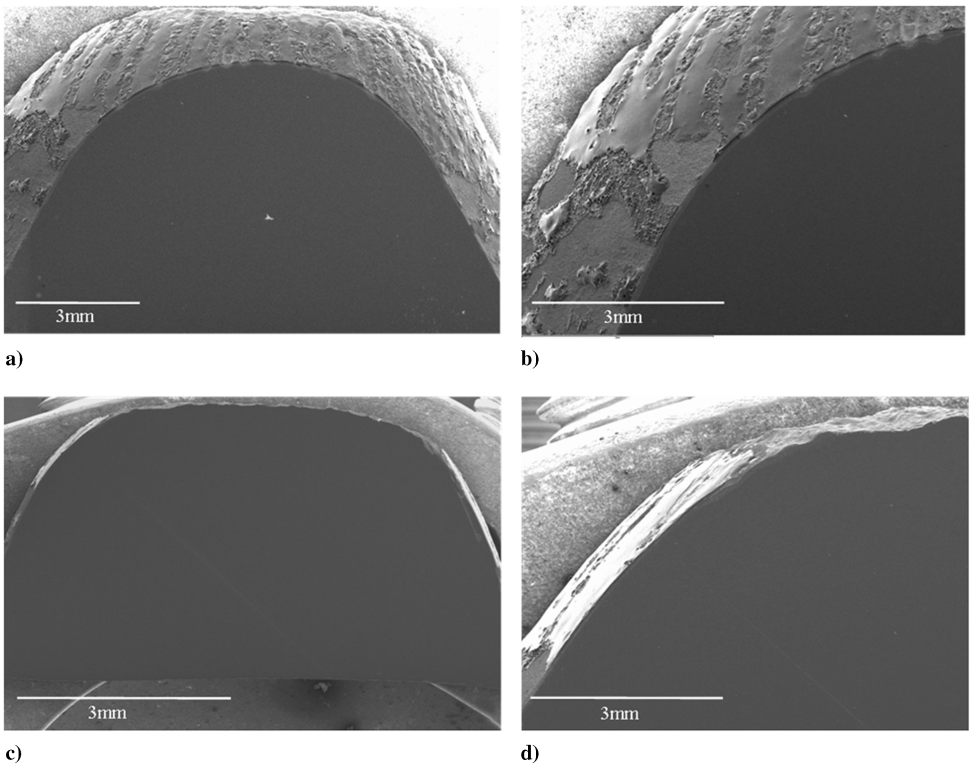

a) b) c) d)

Fig. 6 SEM micrographs: a) of polished cross section 1, b) enlargement of section 1, c) of section 2, and d) enlargement of section 2.

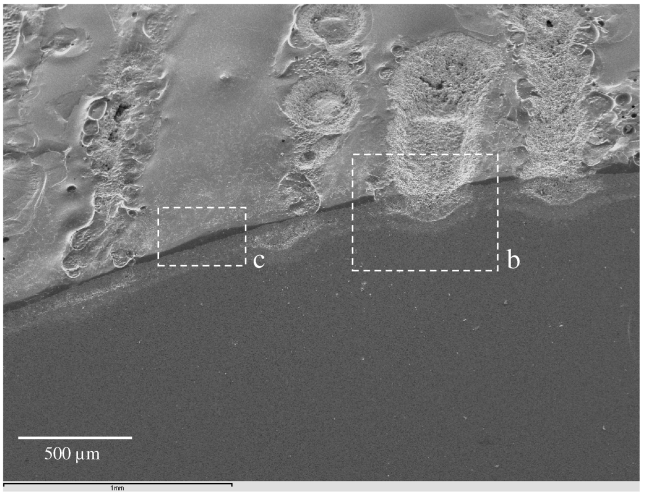

a)

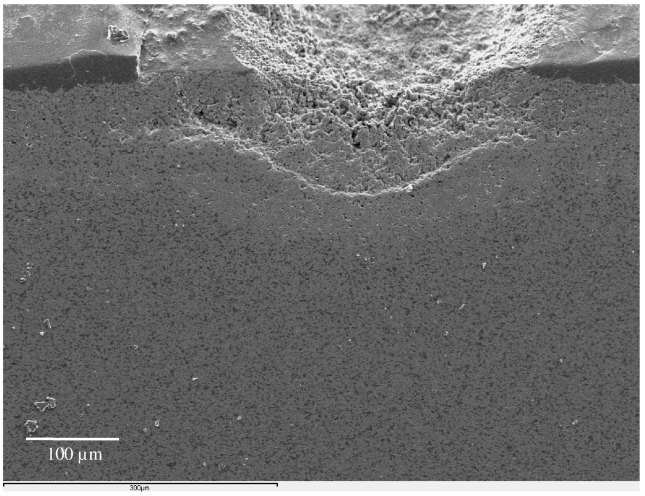

b)

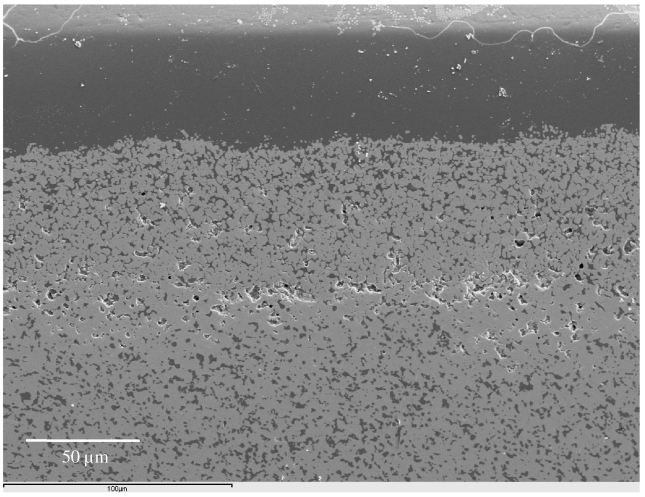

c)

Fig. 7 SEM micrographs: a) from polished cross sections showing with glassy trails: b) magnification of the unprotected zone at the end of a trail, and c) magnification of the protected zone by the silica-based glass layers.

temperature regime favored the active oxidation of SiC. The consumption of SiC created an inner porosity, which is known to represent a major issue for the applicability of this system in extreme environment (see Fig. 8).

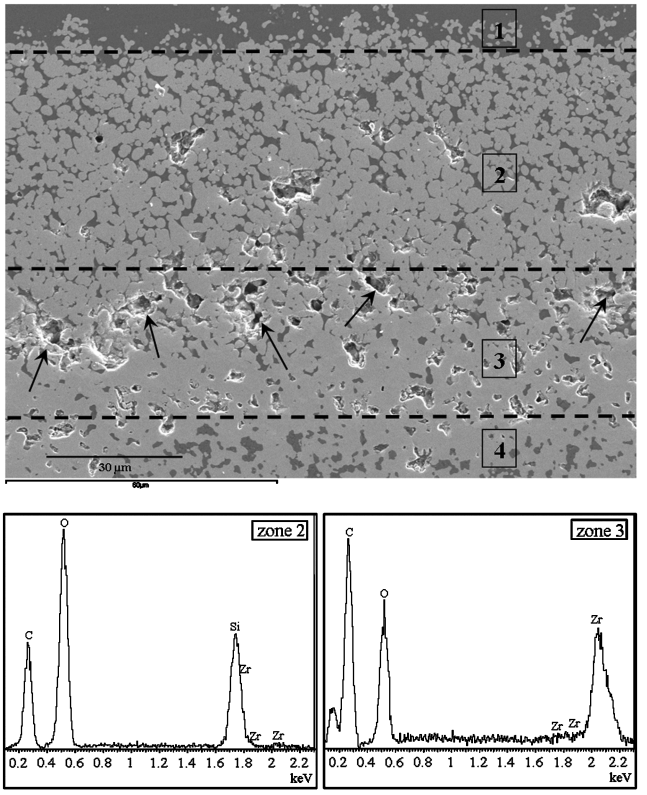

Fig. 8 SEM micrographs from polished cross sections showing protected zones by the silica-based glass and EDS spectra of the regions 2 and 3; region 1: silica-based glassy layer, region 2: oxide layer SiO_2 plus a zirconium reach phase, region 3: SiC-depleted region in which voids are indicated, and region 4: unreacted ZrB_2–SiC.

IV. Numerical Calculations

A systematic numerical analysis was carried out to simulate the environment generated by the plasma torch in order to estimate the material surface catalycity and to relate this evaluation to previous measurements performed at lower temperatures and with a different experimental facility.

The computations were carried out solving the full Navier–Stokes equations for a turbulent multireacting gas mixture with six chemical species (Ar, O, O_2, NO, N, and N_2) in chemical nonequilibrium, according with the Park model [35]. The fluid dynamic equations were numerically solved in the computational domain (plasma torch and test chamber). Convective fluxes were computed according to Roe's flux-difference splitting scheme. Integration of the time-dependent equations was implicit in time until steady state was achieved, solving the linearized system of equations by the multigrid technique. The present code has been extensively validated by numerical experimental correlations and classical numerical benchmarks [36,37].

Because of the relatively long distance between the torch exit and the specimen (6 cm) and to the relatively high pressure, thermal nonequilibrium and electronic species can be neglected in accordance with Kolesnikov et al. [38] despite the high temperature at the exit torch (20,000 K).

According to the calculations, the average specific total enthalpy in proximity of the specimen for the maximum power conditions (63.7 kW, which is the condition at which most of the test has been performed) reduces drastically from the exit torch value of 22 to about 10 MJ/kg (see Fig. 9). The subsonic flow conditions are shown in Fig. 10. At the exit of the torch the plasma containing argon, molecular and atomic nitrogen expands through the nozzle and comes into contact with the surrounding air at ambient conditions, so that oxygen in the atmosphere dissociates and a reacting mixture composed of Ar, O_2, N_2, NO, O, and N is formed. The computed mass fractions for atomic and molecular species with the exception of

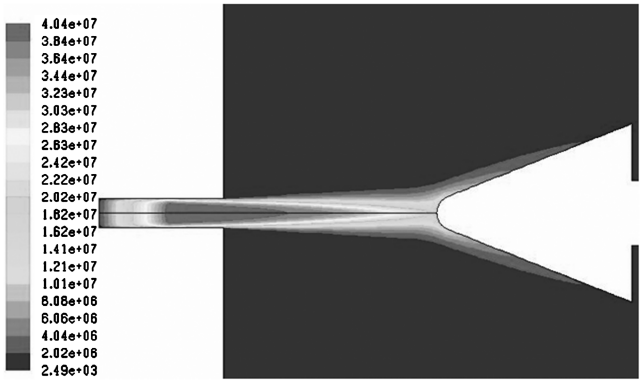

Fig. 9 Contour expressed in J/kg of specific total enthalpy for the case 63.7 kW.

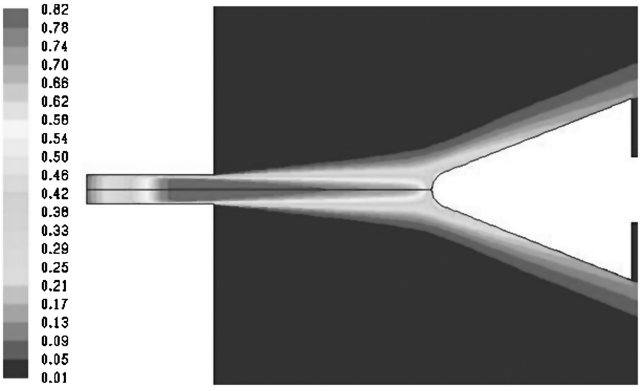

Fig. 10 Contour of Mach number for the case 63.7 kW.

NO, which is negligible (and with noncatalytic wall conditions), are shown in Fig. 11. Near the surface specimen, the concentration of the oxygen and nitrogen molecular increases, while the mass fraction of oxygen and nitrogen atomic decreases. The concentration increasing of N_2 and O_2 is probably due to the reduction of the temperature at almost the same pressure conditions driving to equilibrium composition.

The catalytic activity is commonly described by the recombination coefficient γ, defined as the ratio of the number of dissociating atoms that recombine at the wall to the total number of the colliding atoms with the wall. For a noncatalytic wall, this value is 0, while for a fully catalytic wall, this is 1. The heating of a material's surface because of recombination reactions is determined by the surface energy transfer accommodation coefficient γ', defined as

$$\gamma' = \beta \cdot \gamma \tag{1}$$

where β is the accommodation energy (i.e., the fraction of the energy recombination transferred to the material surface). This parameter is rarely evaluated so that its value is set to unity, although some authors demonstrated that it is often far from 1 [39–42].

Before the extensive computations performed in this work, a preliminary grid-convergence analysis has been carried out to find the best compromise between CPU time and accuracy. Numerical simulations for fully catalytic, cold-wall cases have been performed using meshes with different grid points. The results obtained with the different grids reported in Table 2 show that the computed flowfield is already grid-independent for the mesh with 200×240 grid points. Further increasing the number of grid points gives differences of the computed surface heat fluxes (which are of primary interest in this paper) at the stagnation point of about 1%. The convergence was ensured by reduction of residuals of at least three orders of magnitude and by monitoring the stagnation-point heat fluxes during the iterations. For all the computations after 15,000 iterations, the stagnation-point heat flux does not change significantly ($\ll 0.1\%$).

Numerical computations were carried out under different assumptions about the catalytic properties of the UHTC surface with reference to catalytic efficiency of atomic nitrogen and oxygen. The simulations refers to the plasma torch test conditions.

The catalytic condition at the wall is imposed by a user-defined function that establishes the wall species mass fraction by the diffusive-flux condition:

$$\rho\alpha|_w K_w(T_w) = \rho D\bar{\nabla}\alpha \cdot \bar{n} \tag{2}$$

The relationship between the catalytic constant and accommodation coefficient γ' is

$$K_w = \gamma' \sqrt{\frac{R_0 T_w}{2\pi M}} \tag{3}$$

Reynolds number referred to the exit torch diameter is estimated to be in the range of 5000–10,000. Typically, for the turbulent Schmidt number,

$$Sc_t = \frac{\mu_t}{\rho D_t} \tag{4}$$

where a value of 0.7 is used in equilibrium or fully catalytic flowfield calculations. In the present computations in a finite catalytic environment, the Sc_t value directly affects diffusion; therefore, a sensitivity analysis on the Sc_t has been carried out in order to assess the effect of this parameter on the results. Sc_t has been changed between 0.1 and 1. Figure 12 shows the normalized surface heat fluxes with the stagnation-point value for $Sc_t = 1$ in order to underline the differences. Also, considering a differences of 20% in the surface heat fluxes (obtained between $Sc_t = 1$ and $Sc_t = 0.1$), a difference lower than 5% is obtained in terms of temperature (i.e., the numerical point for finite catalycity in Fig. 13 should be shifted down about 100 K, which does not affect the following discussion).

Based on the computed heat-flux distributions, assuming a turbulent Schmidt number of 0.7, a thermal analysis was carried out

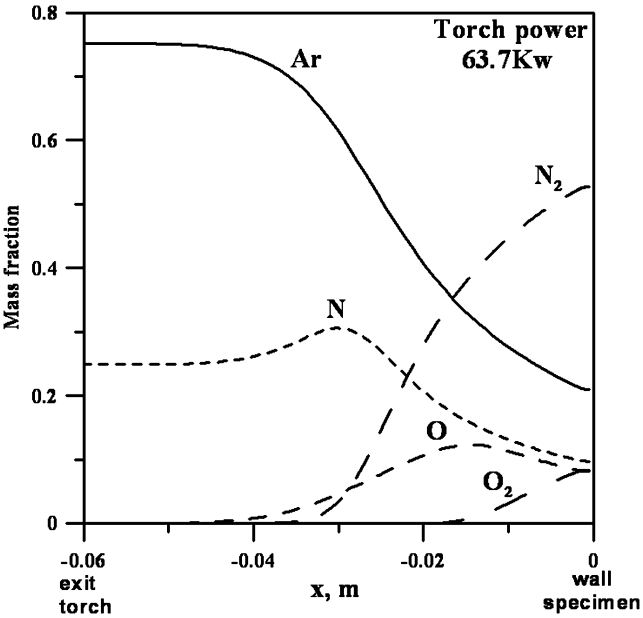

Fig. 11 Mass fraction profiles of 63.7 kW case; total enthalpy: 1) torch exit: 22 MJ/kg and 2) in front of the specimen: 10 MJ/kg.

Table 2 Computational grid

Grid	Stagnation-point heat flux, MW/m^2
100×120	27.8
200×240	26.5
400×480	26.2

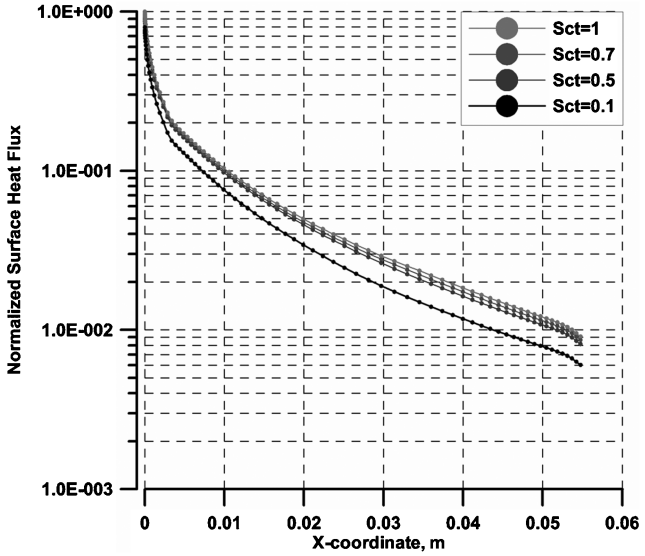

Fig. 12 Normalized stagnation-point heat flux for different Sc_t.

to evaluate the γ' value needed to fit the experimental temperature data. Figure 13 shows the steady-state results computed under the two assumptions of fully catalytic and noncatalytic wall and the experimental data obtained with the pyrometer for both material samples. For thermal analysis, input values of density, specific heat, and thermal conductivity are necessary. The values for the ZrB_2–SiC material were taken from previous characterization performed on the same composition: 5.61 $g\,cm^{-3}$, 628 $J\,kg^{-1}\,K^{-1}$, and 66 $W\,m^{-1}\,K^{-1}$ [43]. Only the specific heat variation of ZrB_2/SiC with temperature was available (from 450 to 810 J/kg K and from 300 to 2200 K). An average value of 628 J/kg K has been used in the computations to ease the computational load; in any case, this assumption does not affect the final steady-state result too much (the transient was not of interest).

The experimental results are slightly higher than numerical values corresponding to the noncatalytic wall condition. Indeed, at 2300°C (i.e., at the maximum temperature reached during the plasma test), the estimated value for γ' is about 10^{-4}. This result indicates that the external deposit of zirconia formed for oxidation during the plasma

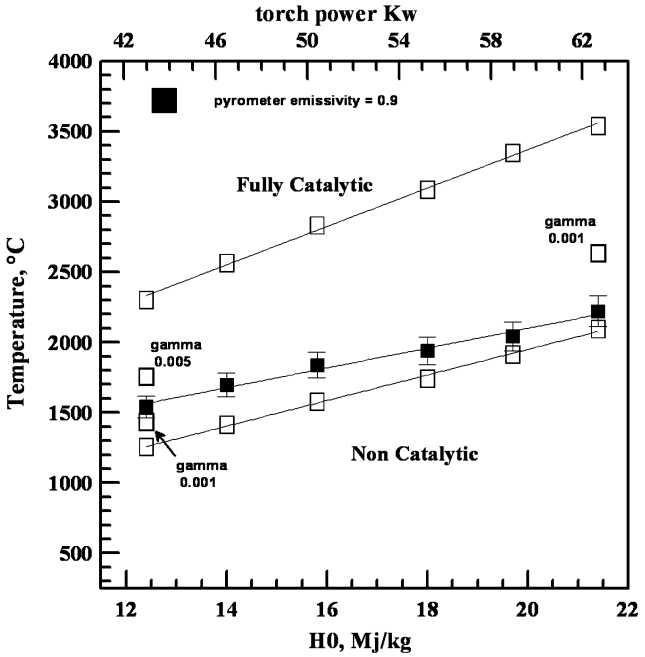

Fig. 13 Maximum temperatures for catalytic and noncatalytic case and for the actual test.

test has a very low catalytic activity at high temperatures. Combining the value of γ' with the values of the atomic oxygen recombination coefficient γ for sintered zirconia stabilized with yttria (Y_2O_3), evaluated by Balat-Pichelin et al. [44] by a direct method [45], the value of the accommodation energy β for this class of ceramics is about 5×10^{-4} at 2200°C. The estimation of β is considered to be preliminary because the recombination coefficient γ used is related only to the atomic oxygen recombination and, moreover, its measurement was not performed.

It is important to note that when increasing the specific total enthalpy, the temperature in the region close to the wall increases and therefore the level of dissociation increases; this does not lead to a higher catalytic activity. It has to be kept in mind that the evaluation performed in this work concerns the γ', which is the product of the recombination coefficient γ and the accommodation energy β. Direct measurements of γ on this material showing an increase of γ with the temperature are available [26], but these data are only up to 1800 K. At higher temperatures, the surface modifications are radically different; therefore, no simple extrapolation of the gamma behavior can be done at this point. Moreover, the dependence of β with T is not really clear. The experimental data and the numerical simulation reported in this work simply show that at the highest enthalpies, and therefore at the highest surface temperature, the catalytic property of the material are reduced, and this may be attributed to the surface oxidation.

Further measurements of γ and γ' taken in the same experimental conditions are needed in order to have a more reliable evaluation of the accommodation energy and confirm the preliminary conclusions reported here.

V. Conclusions

An ultra-high-temperature ZrB_2–SiC ceramic nose cone produced by EDM out of a hot-pressed billet was tested in a plasma torch facility for 10 min at temperatures above 2000°C.

The posttest inspection of the model after exposure showed a nonnegligible surface erosion; nonetheless, the material has a promising potential to withstand extremely severe oxidizing conditions with temperatures exceeding 2000°C in a single-use application. There still remain issues on the actual applicability of UHTC-based components to the manufacturing of complex hot structures: because the fact that, given the low thermal shock resistance of monolithic ceramics, only small parts can be produced reliably, and this poses the problem of the backwall high temperature and of the mechanical interfaces with other ceramic matrix composites or metal. This issue is currently being addressed in dedicated technological national projects conducted by Centro Italiano Ricerche Aerospaziali and the Italian Space Agency. However, the results obtained at material level in this experimental work represent a promising starting point on the potential of this class of ceramics.

The numerical calculations simulated the chemical nonequilibrium flow around the model assuming a low catalytic surface behavior. The calculated results are in good accordance with the experimental ones, allowing to conclude that the nose cone constituent material is characterized by extremely low surface catalycity. Real-time spectral directional emissivity measurements showed a high-radiative efficiency with emissivity values close to 0.9.

Acknowledgments

The authors wish to thank Raffaele Savino (University of Naples "Federico II," Department of Aerospace Engineering) and Mario Tului (Centro Sviluppo Materiali, Rome) for their kind contribution to this work.

References

[1] Cutler, R. A., "Engineering Properties of Borides," *Engineered Materials Handbook: Ceramics and Glasses*, edited by S. J. Schneider Jr., Vol. 4, CRC Press, Boca Raton, FL, 1991, pp. 787–803.

[2] Gasch, M. J., Ellerby, D. T., and Johnson, S. M., "Ultra High Temperature Ceramic Composites," *Handbook for Glass, Ceramics*

and Composites, ASTM International, West Conshohocken, PA, 2004.

[3] Monteverde, F., and Savino, R., "Stability of Ultra-High-Temperature ZrB_2–SiC Ceramics Under Simulated Atmospheric Re-Entry Conditions," *Journal of the European Ceramic Society*, Vol. 27, No. 16, 2007, pp. 4797–4805. doi:10.1016/j.jeurceramsoc.2007.02.201

[4] Van Wie, D. M., Drewy, D. G., Jr., King, D. E., and Hudson, C. M., "The Hypersonic Environment: Required Operating Conditions and Design Challenges," *Journal of Materials Science*, Vol. 39, No. 19, 2004, pp. 5915–5924. doi:10.1023/B:JMSC.0000041688.68135.8b

[5] Opeka, M. M., Talmy, I. G., and Zaykoski, J. A., "Oxidation-Based Materials Selection for 2000°C+ Hypersonic Aerosurfaces: Theoretical Considerations and Historical Experience," *Journal of Materials Science*, Vol. 39, No. 19, 2004, pp. 5887–5904. doi:10.1023/B:JMSC.0000041686.21788.77

[6] Chamberlain, A., Fahrenholtz, W., Hilmas, G., and Ellerby, D., "Oxidation of ZrB_2–SiC Ceramics Under Atmospheric and Reentry Conditions," *Refractories Applications and News*, Vol. 1, No. 2, 2005, pp. 1–8.

[7] Kolodziej, P., Salute, J., and Keese, D. L., "First Flight Demonstration of a Sharp Ultra-High Temperature Ceramic Nosetip," NASA TM-112215, Dec. 1997.

[8] Smith, D., Caroll, C., Marschall, J., and Pallix, J., "Materials Testing on the DC-X and DC-XA," NASA TM-110430, Jan. 1997.

[9] Kuriakose, A. K., and Margrave, J. L., "The Oxidation Kinetics of Zirconium Diboride and Zirconium Carbide at High Temperatures," *Journal of the Electrochemical Society*, Vol. 111, No. 7, 1964, pp. 827–831. doi:10.1149/1.2426263

[10] Tripp, W. C., and Graham, H. C., " Thermogravimetric Study of the Oxidation of ZrB_2 in the Temperature Range of 800°C to 1500°C," *Journal of the Electrochemical Society*, Vol. 118, No. 7, 1971, pp. 1195–1199. doi:10.1149/1.2408279

[11] Opeka, M. M., Talmy, I. G., Wuchina, E. J., Zaykoski, J. A., and Causey, S. J., "Mechanical, Thermal, and Oxidation Properties of Refractory Hafnium and Zirconium Compounds," *Journal of the European Ceramic Society*, Vol. 19, No. 13, 1999, pp. 2405–2414. doi:10.1016/S0955-2219(99)00129-6

[12] Fahrenholtz, W. G., Hilmas, G. E., Chamberlain, A. L., and Zimmermann, J. W., "Processing and Characterization of ZrB_2-Based Ultra-High Temperature Monolithic and Fibrous Monolithic Ceramics," *Journal of Materials Science*, Vol. 39, No. 19, 2004, pp. 5951–5957. doi:10.1023/B:JMSC.0000041691.41116.bf

[13] Fahrenholtz, W. G., "The ZrB_2 Volatility Diagram," *Journal of the American Ceramic Society*, Vol. 88, No. 12, 2005, pp. 3509–3512. doi:10.1111/j.1551-2916.2005.00599.x

[14] Levine, S. R., Opila, E. J., Halbig, M. C., Kiser, J. D., Singh, M., and Salem, J. A., "Evaluation of Ultra-High Temperature Ceramics for Aeropropulsion Use," *Journal of the European Ceramic Society*, Vol. 22, Nos. 14–15, 2002, pp. 2757–2767. doi:10.1016/S0955-2219(02)00140-1

[15] Ban'kovskaya, I. B., and Zhabrev, V. A.," Kinetic Analysis of the Heat Resistance of ZrB_2–SiC Composites," *Glass Physics and Chemistry*, Vol. 31, No. 4, 2005, pp. 482–488. doi:10.1007/s10720-005-0087-8

[16] Rezaie, A., Fahrenholtz, W. G., and Hilmas, G. E., "Evolution of Structure During the Oxidation of Zirconium Diboride–Silicon Carbide in Air up to 1500°C," *Journal of the European Ceramic Society*, Vol. 27, No. 6, 2007, pp. 2495–2501. doi:10.1016/j.jeurceramsoc.2006.10.012

[17] Fahrenholtz, W. G., "Thermodynamic Analysis of ZrB_2–SiC Oxidation, Formation of a SiC-Depleted Region," *Journal of the American Ceramic Society*, Vol. 90, No. 1, 2007, pp. 143–148. doi:10.1111/j.1551-2916.2006.01329.x

[18] Han, J., Hu, P., Zhang, X., and Meng, S., "Oxidation Behavior of Zirconium Diboride–Silicon Carbide at 1800°C," *Scripta Materialia*, Vol. 57, No. 9, 2007, pp. 825–828. doi:10.1016/j.scriptamat.2007.07.009

[19] Opila, E. J., Levine, S. R., and Lorincz, J. A., "Oxidation of ZrB_2- and HfB_2-Based Ultra-High Temperature Ceramics: Effect of Ta Additions," *Journal of Materials Science*, Vol. 39, No. 19, 2004, pp. 5969–5977. doi:10.1023/B:JMSC.0000041693.32531.d1

[20] Gasch, M., Ellerby, D., Irby, E., Beckman, S., Gusman, M., and Johnson, S., "Processing, Properties and Arc Jet Oxidation of Hafnium Diboride/Silicon Carbide Ultra High Temperature Ceramics," *Journal of Materials Science*, Vol. 39, No. 19, 2004, pp. 5925–5937. doi:10.1023/B:JMSC.0000041689.90456.af

[21] Han, J., Hu, P., Zhang, X., Meng, S., and Han, W., "Oxidation-Resistant ZrB_2–SiC Composites at 2200°C," *Composites Science and Technology*, Vol. 68, Nos. 3–4, 2008, pp. 799–806. doi:10.1016/j.compscitech.2007.08.017

[22] Russo, G., and Marino, G., "The USV Program and UHTC Development," *Proceedings of 4th European Workshop on Thermal Protection Systems for Space Vehicles*, ESA, Paris, 2002, pp. 157–163.

[23] Scatteia, L., Del Vecchio, A., De Filippis, F., Marino, G., and Savino, R., "PRORA-USV SHS: Development of Sharp Hot Structures Based on Ultra High Temperature Metal Diborides Current Status," *Proceedings of 56th International Astronautical Congress*, International Astronautical Federation, Paris, Oct. 2005.

[24] Monteverde, F., Bellosi, A., and Scatteia, L., "Processing and Properties of Ultra-High Temperature Ceramics for Space Applications," *Materials Science and Engineering: A*, Vol. 485, Nos. 1–2, 2008, pp. 415–421. doi:10.1016/j.msea.2007.08.054

[25] Monteverde, F., and Scatteia, L., "Resistance to Thermal Shock and to Oxidation of Metal Diborides–SiC Ceramics for Aerospace Application," *Journal of the American Ceramic Society*, Vol. 90, No. 4, 2007, pp. 1130–1138. doi:10.1111/j.1551-2916.2007.01589.x

[26] Scatteia, L., Borrelli, R., Cosentino, G., Bêche, E., Sans, J. L., and Balat-Pichelin, M., "Catalytic and Radiative Behaviors of ZrB_2–SiC Ultra High Temperature Ceramic Composites," *Journal of Spacecraft and Rockets*, Vol. 43, No. 5, 2006, pp. 1004–1012. doi:10.2514/1.21156

[27] Scatteia, L., Alfano, D., Monteverde, F., Sans, J. L., and Balat-Pichelin, M., "Effect of Machining Method on the Catalycity and Emissivity of ZrB_2 and ZrB_2–HfB_2-Based Ceramics," *Journal of the American Ceramic Society*, Vol. 91, No. 5, 2008, pp. 1461–1468. doi:10.1111/j.1551-2916.2008.02325.x

[28] Savino, R., De Stefano Fumo, M., Silvestroni, L., and Sciti, D., "Arcjet Testing on HfB_2 and HfC-Based UHTC Materials," *Journal of the European Ceramic Society*, Vol. 28, No. 9, 2008, pp. 1899–1907. doi:10.1016/j.jeurceramsoc.2007.11.021

[29] De Stefano Fumo, M., Savino, R., Paterna, D., Di Maso, A., and Monteverde, F., "Analysis and Design of Ultra High Temperature Ceramics Hot Structures for Ground and Flight Tests," *6th European Workshop on Thermal Protection Systems and Hot Structures*, ESA, Paris, 1–3 April 2009.

[30] Heuer, A. H., and Lou, V. L. K., "Volatility Diagrams for Silica, Silicon Nitride, and Silicon Carbide and Their Application to High-Temperature Decomposition and Oxidation," *Journal of the American Ceramic Society*, Vol. 73, No. 10, 1990, pp. 2789–2803. doi:10.1111/j.1151-2916.1990.tb06677.x

[31] Schneider, B., Guette, A., Naslain, R., Cataldi, M., and Costecalde, A., "A Theoretical and Experimental Approach to the Active-to-Passive Transition in the Oxidation of Silicon Carbide: Experiments at High Temperatures and Low Total Pressures," *Journal of Materials Science*, Vol. 33, No. 2, 1998, pp. 535–547. doi:10.1023/A:1004313022769

[32] Jacobson, N. S., "Corrosion of Silicon-Based Ceramics in Combustion Environments," *Journal of the American Ceramic Society*, Vol. 76, No. 1, 1993, pp. 3–28. doi:10.1111/j.1151-2916.1993.tb03684.x

[33] Balat, M. J. H., "Determination of the Active-to-Passive Transition in the Oxidation of Silicon Carbide in Standard and Microwave-Excited Air," *Journal of the European Ceramic Society*, Vol. 16, No. 1, 1996, pp. 55–62. doi:10.1016/0955-2219(95)00104-2

[34] Morino, Y., Yoshinaka, T., Auweter-Kurtz, M., Hilfer, G., Speckmann, H.-D., and Sakai, A., "Erosion Characteristics of SiC Coated C/C Materials in Arc-Heated High Enthalpy Air Flow," *Acta Astronautica*, Vol. 50, No. 3, 2002, pp. 149–158. doi:10.1016/S0094-5765(01)00150-3

[35] Park, C., "Review of Chemical-Kinetic Problems of Future NASA Missions: 1. Earth Entries," *Journal of Thermophysics and Heat Transfer*, Vol. 7, No. 3, 1993, pp. 385–398. doi:10.2514/3.431

[36] Paterna, D., Monti, R., Savino, R., and Esposito, A., "Experimental and Numerical Investigation of Martian Atmosphere Entry," *Journal of Spacecraft and Rockets*, Vol. 38, No. 6, 2001, pp. 1–10.

[37] Savino, R., and De Stefano Fumo, M., "Aerothermodynamic Analyses of a Sharp Ultraghigh-Temperature Winglet for Atmospheric Reentry Flight Tests," *Journal of Thermophysics and Heat Transfer*, Vol. 22, No. 4, 2008, pp. 669–676.

doi:10.2514/1.33296

[38] Kolesnikov, A. F., Yakushin, M. I., Pershin, I. S., Vasilevskii, S. A., Chaot, O., and Vancrayenest, B., "Comparative Study of Surface Catalyticity Under Subsonic Air Test Conditions," *Proceedings of the 4th European Symposium Aerothermodynamics for Space Vehicles*, ESA, Paris, 2001, pp. 481–486.

[39] Halpern, B., and Rosner, D. E., "Chemical Energy Accommodation at Catalyst Surfaces," *Transactions of the Faraday Society*, Vol. 74, No. 8, 1978, pp. 1883–1912.

[40] Melin, G. A., and Madix, R. J., "Energy Accommodation During Oxygen Atom Recombination on Metal Surfaces," *Transactions of the Faraday Society*, Vol. 67, 1971, pp. 198–211. doi:10.1039/tf9716700198

[41] Carleton, K. L., and Marinelli, W. J., "Spacecraft Thermal Energy Accommodation from Atomic Recombination," *Journal of Thermophysics and Heat Transfer*, Vol. 6, No. 4, 1992, pp. 650–655. doi:10.2514/3.11547

[42] Clark, R. K., Cunnington, G. R., and Robinson, J. C., "Vapor-Deposited Emittance-Catalysis Coatings for Superalloys in Heat-Shield Applications," *Journal of Thermophysics and Heat Transfer*, Vol. 1, No. 1, 1987, pp. 28–34. doi:10.2514/3.4

[43] Alfano, D., "Database for Qualification Model," Centro Italiano Ricerche Aerospaziali Rept. CF-07-0067, Capua, Italy, 2007.

[44] Balat-Pichelin, M., Badie, J. M., Berjoan, R., and Boubert, P., "Recombination Coefficient of Atomic Oxygen on Ceramic Materials Under Earth Re-Entry Conditions by Optical Emission Spectroscopy," *Chemical Physics*, Vol. 291, No. 2, 2003, pp. 181–194. doi:10.1016/S0301-0104(03)00152-6

[45] Balat-Pichelin, M., Passarelli, M., Scatteia, L., and Alfano, D., "Catalycity of Zirconia and ZrB_2-Based Ultra-High Temperature Ceramics," *Proceedings of 6th European Symposium on Aerothermodynamics for Space Vehicles*, ESA, Paris (to be published).

T. Lin
Associate Editor